Supplementary Information for:

Self-generated gradients steer collective migration on viscoelastic collagen networks

Andrew G. Clark[1,10,11,✉], Ananyo Maitra[2,3,✉], Cécile Jacques[1], Martin Bergert[4], Carlos Pérez-González[1], Anthony Simon[1], Luc Lederer[1], Alba Diz-Muñoz[4], Xavier Trepat[5,6,7,8], Raphaël Voituriez[3,9,12] and Danijela Matic Vignjevic[1,12]

[1] *Cell Biology and Cancer Unit, Institut Curie, PSL Research University, Paris, France.*

[2] *Laboratoire Jean Perrin, Sorbonne Université and CNRS, Paris, France.*

[3] *Laboratoire de Physique Théorique et Modélisation, CNRS, CY Cergy Paris Université, Cergy-Pontoise Cedex, France*

[4] *Cell Biology and Biophysics Unit, European Molecular Biology Laboratory, Heidelberg, Germany*

[5] *Institute for Bioengineering of Catalonia, The Barcelona Institute for Science and Technology (BIST), Barcelona, Spain.*

[6] *Facultat de Medicina, University of Barcelona, Barcelona, Spain.*

[7] *Institució Catalana de Recerca i Estudis Avançats (ICREA), Barcelona, Spain.*

[8] *Centro de Investigación Biomédica en Red en Bioingeniería, Biomateriales y Nanomedicina, Barcelona, Spain.*

[9] *Laboratoire de Physique Théorique de la Matière Condensée, Sorbonne Université and CNRS, Paris, France.*

[10] *Present Address: Institute of Cell Biology and Immunology, Stuttgart Research Center Systems Biology, University of Stuttgart, Stuttgart, Germany*

[11] *Present Address: Center for Personalized Medicine, University of Tübingen, Tübingen, Germany.*

[12] *These authors contributed equally to this work: Raphaël Voituriez, Danijela Matic Vignjevic*

✉*email: andrew.clark@srcsb.uni-stuttgart.de; nyomaitra07@gmail.com.*

Contents

Supplementary Video Captions

Supplementary Video 1. A431 cluster migrating on a 0.5kPa PAA gel coated with a thin collagen-I network. Scale Bar: 100μm. HH:MM.

Supplementary Video 2. A431 cluster migrating on a 0.5kPa PAA gel coated with 100μg/ml monomeric collagen-I. Scale Bar: 100μm. HH:MM.

Supplementary Video 3. A431 myosin light chain (MLC)-GFP clusters migrating on collagen-I networks. Magenta lines indicate region used for segmentation of the cluster cortex. Scale Bar: 50μm. HH:MM.

Supplementary Video 4. A431 cluster migrating on a fluorescently-labeled collagen network. *Left*: the fluorescent collagen is shown in pseudocolor and the cell outline is shown in white. The white dot represents the cluster center of mass. Scale Bar: 50μm. HH:MM. *Right*: Separation of the segmentation into equal-length segments from front (yellow) to rear (purple).

Supplementary Video 5. Rapid removal of an A431 cell cluster on a fluorescent collagen network. *Left*: Brightfield. *Middle*: Collagen in grayscale with cluster segmentation in magenta. *Right*: Collagen in grayscale with vectors from PIV shown in colors according to angle. Time 0:00 refers to frame prior to addition of Trypsin/NH_4OH. Subsequent timestamps refer to time after Trypsin/NH_4OH treatment. Scale Bar: 50μm. Scale Vector: 0.5μm/min. HH:MM.

Supplementary Video 6. 3D displacement microscopy experiment for an A431 cell cluster on a

collagen network and rapidly removed using Trypsin/NH_4OH. Black arrows: *xy* displacement vectors. Color scale: *z* displacement vectors (negative values indicate displacement down toward the substrate). Time 0:00 refers to frame prior to addition of Trypsin/NH_4OH. Subsequent timestamps refer to time after Trypsin/NH_4OH treatment. Scale Bar: 50μm. Scale Vector: 50μm. HH:MM.

Supplementary Video 7. A431 cluster detaching from a collagen-I network following treatment with 10μg/ml AIIB2. Scale Bar: 100μm. HH:MM.

Supplementary Video 8. Rapid removal of an A431 cell cluster on a fluorescent collagen network crosslinked with 1mM threose. *Left*: Brightfield. *Middle*: Collagen in grayscale with cluster segmentation in magenta. *Right*: Collagen in grayscale with vectors from PIV shown in colors according to angle. Time 0:00 refers to frame prior to addition of Trypsin/NH_4OH. Subsequent timestamps refer to time after Trypsin/NH_4OH treatment. Scale Bar: 50μm. Scale Vector: 0.5μm/min. HH:MM.

Supplementary Video 9. Rapid removal of an A431 cell cluster on a fluorescent collagen network crosslinked with 10mM threose. *Left*: Brightfield. *Middle*: Collagen in grayscale with cluster segmentation in magenta. *Right*: Collagen in grayscale with vectors from PIV shown in colors according to angle. Time 0:00 refers to frame prior to addition of Trypsin/NH_4OH. Subsequent timestamps refer to time after Trypsin/NH_4OH treatment. Scale Bar: 50μm. Scale Vector: 0.5μm/min. HH:MM.

Supplementary Video 10. Rapid removal of an A431 cell cluster on a fluorescent collagen net-

work crosslinked with 0.05% glutaraldehyde. *Left*: Brightfield. *Middle*: Collagen in grayscale with cluster segmentation in magenta. *Right*: Collagen in grayscale with vectors from PIV shown in colors according to angle. Time 0:00 refers to frame prior to addition of Trypsin/NH_4OH. Subsequent timestamps refer to time after Trypsin/NH_4OH treatment. Scale Bar: 50μm. Scale Vector: 0.5μm/min. HH:MM.

Supplementary Video 11. A431 cluster migrating on a fluorescently-labeled collagen network crosslinked with 1mM threose. *Left*: the fluorescent collagen is shown in pseudocolor and the cell outline is shown in white. The white dot represents the cluster center of mass. Scale Bar: 50μm. HH:MM. *Right*: Separation of the segmentation into equal-length segments from front (yellow) to rear (purple).

Supplementary Video 12. A431 cluster migrating on a fluorescently-labeled collagen network crosslinked with 10mM threose. *Left*: the fluorescent collagen is shown in pseudocolor and the cell outline is shown in white. The white dot represents the cluster center of mass. Scale Bar: 50μm. HH:MM. *Right*: Separation of the segmentation into equal-length segments from front (yellow) to rear (purple).

Supplementary Video 13. A431 cluster migrating on a fluorescently-labeled collagen network crosslinked with 0.05% glutaraldehyde. *Left*: the fluorescent collagen is shown in pseudocolor and the cell outline is shown in white. The white dot represents the cluster center of mass. Scale Bar: 50μm. HH:MM. *Right*: Separation of the segmentation into equal-length segments from front (yellow) to rear (purple).

Supplementary Video 14. A431 cluster migrating on a collagen-I network. Scale Bar: 100μm. HH:MM.

Supplementary Video 15. A431 cluster migrating on a collagen-I network crosslinked with 1mM threose. Scale Bar: 100μm. HH:MM.

Supplementary Video 16. A431 cluster migrating on a collagen-I network crosslinked with 10mM threose. Scale Bar: 100μm. HH:MM.

Supplementary Video 17. A431 cluster migrating on a collagen-I network crosslinked with 0.05% glutaraldehyde. Scale Bar: 100μm. HH:MM.

Supplementary Video 18. Rapid removal of an individual A431 cell on a fluorescent collagen network. *Left*: Brightfield. *Middle*: Collagen in grayscale with cluster segmentation in magenta. *Right*: Collagen in grayscale with vectors from PIV shown in colors according to angle. Time 0:00 refers to frame prior to addition of Trypsin/NH_4OH. Subsequent timestamps refer to time after Trypsin/NH_4OH treatment. Scale Bar: 50μm. Scale Vector: 0.5μm/min. HH:MM.

Supplementary Video 19. A431 single cell migrating on a fluorescently-labeled collagen network. *Left*: the fluorescent collagen is shown in pseudocolor and the cell outline is shown in white. The white dot represents the cluster center of mass. Scale Bar: 50μm. HH:MM. *Right*: Separation of the segmentation into equal-length segments from front (yellow) to rear (purple).

Supplementary Video 20. A431 single cell migrating on a collagen-I network. Scale Bar: 50μm.

HH:MM.

Supplementary Video 21. A431 clusters migrating on a 0.5kPa PAA gel coated with a thin collagen-I network analyzed by traction force microscopy. Arrows: *xy* traction stresses on the substrate. Scale Bar: 100μm. Scale Vector: 50Pa. HH:MM.

Supplementary Video 22. A431 cells stably expressing mCherry-LifeAct overlaid with vectors from PIV analysis of actin flows in the peripheral cortical region. Scale bar: 20μm. Scale vector: 0.05μm/min. MM:SS.

Supplementary Discussion

The role of substrate deformation during cell migration has been studied extensively using purely elastic PAA substrates[24,41,65,66]. Recent work comparing cell spreading and migration on elastic vs. viscoelastic PAA substrates found that some cell types can migrate faster and more persistently on viscoelastic substrates[46,47,67], consistent with our findings for cell cluster migration. Our study provides a mechanism for these findings, namely that increased relaxation time in viscoelastic substrates can lead to asymmetric substrate deformations during migration, which in turn drive persistent migration. This mechanism is similar in spirit to a model showing that apolar colloidal particles can become spontaneously self-propelled and swim in a highly persistent fashion as a result of changes in local solute concentrations due to hydrodynamic flows during particle motion[39].

Spontaneous persistent migration has recently been observed for cells migrating in uniform concentrations of chemokine by self-generated chemotaxis[68,40]. Because cells consume chemoattractant as they migrate, chemokine is depleted at the cell rear and remains highly concentrated at the cell front, effectively creating a sharp local chemokine gradient. This is similar to our mechanism in that local changes to the substrate/chemokine field during migration creates a polarity cue to continue migrating along the same direction. The finite diffusion of chemokine during self-generated chemotaxis is analogous to substrate relaxation time in our model.

Recent work has shown that small groups of cells, similar to the clusters presented in this study, can collectively migrate up chemokine gradients, and that collective behavior may offer advantages in gradient sensing during chemotaxis[49,50]. Collective chemotaxis is controlled by polarized

contractile myosin at the cluster rear, which drives intra-cluster cell flows down the cluster sides and rear and up the middle of the cluster[50]. Another recent study has reported the formation of transient substrate stiffness gradients that drive durotaxis of neural crest cells during *Xenopus* development[43]. These traveling gradients require interactions between the neural crest cells and underlying placodal layer and are dependent on cadherin-based cell-cell interactions, cell-ECM adhesions and polarized Rac and actomyosin activity. Polarized Rac activity is also known to be crucial for *Drosophila* border cell migration[69]. In our study, persistent collective migration occurs spontaneously and in the absence of asymmetric distributions of myosin or Rac activity (Extended Data Fig. 3a, b) or cell rearrangements within the cluster (Extended Data Fig. 1a, b) and relies rather on the physical interactions between the cluster and its substrate. It is likely, however, that the epithelial polarity mechanisms involved in keeping cell clusters together are required, as well as regulation of myosin-2 activity, as the loss of these mechanisms lead to dissolution of the cell clusters into individual cells[23] (Extended Data Fig. 10f).

Deposition of new ECM during migration has recently been shown to play a role in controlling cell migration persistence[70]. A431 cells have previously been shown to secrete ECM proteins such as collagen-IV and laminin[71]. However, we did not find evidence of local ECM deposition on collagen networks during collective migration (Extended Data Fig. 6a-c). Although we did detect fibronectin decorating collagen fibers, fibronectin is present in fetal bovine serum (FBS) and can readily adsorb onto collagen networks[72]. In line with this, we observed fibronectin present on collagen networks even in the absence of cell clusters (Extended Data Fig. 6a). Fibronectin staining appeared identical in the presence of cell clusters, and we did not observe any radial gradient in

fibronectin across the cluster radius (Extended Data Fig. 6b). To better characterize the cell-ECM interactions, we treated clusters with the specific integrin binding inhibitors Cilengitide, a specific inhibitor of integrin-αvβ3/5 (RGD binding, e.g. Fibronectin)[73] and AIIB2, a functional antibody that distrupts integrin-β1 (collagen binding)[74]. While clusters treated with Cilengitide did not have altered migration, clusters treated with AIIB2 appeared to migrate more slowly and less persistently (Extended Data Fig. 5c). However, treatment with AIIB2 led to the rapid retraction of cell protrusions and cluster rounding. Clusters remained loosely attached to the collagen networks for several hours, moving in a diffusive manner before detaching (Extended Data Fig. 5d, Supplementary Video 7), suggesting that the observed differences in migration speed and persistence likely do not reflect changes in active migration, but rather a passive diffusive behavior.

In our study, we find that cell clusters generate local gradients in collagen density, collagen stiffness and nematic alignment of collagen fibers. Clusters migrate down the gradients of density and stiffness and up the alignment gradient. This may seem counterintuitive in light of numerous studies that have identified mechanisms of durotaxis, where cells or groups of cells migrate up imposed stiffness gradients[41–43,75,76]. However, it is difficult to directly compare results from imposed gradients with the dynamic self-generated gradients we observe on collagen networks, as the motility mechanisms in the two cases are likely to be distinct. In addition, negative durotaxis, or migration toward softer substrates, has also recently been observed *in vitro* and *in vivo*, namely during axonal migration in the developing *Xenopus* brain[44,45]. Gradients in collagen density and stiffness could also influence the effective friction along the gradient axis. Higher friction at the cluster rear resulting from higher collagen density could, for example, contribute to the bias to-

ward rearward-directed actin flows and influence protrusion formation/stability, which we observe to be favored at the cluster front. In a recent model of negative durotaxis, higher actin flows in protrusions directed down the stiffness gradient were linked to increased extension and decreased retraction rates[45], consistent with our observations of protrusion bias toward the cluster front.

The observation that cell clusters move up collagen alignment gradients is perhaps more intuitive: because the minimum in collagen alignment is shifted toward the rear, this could favor protrusion formation along the aligned fibers at the cluster front and thereby promote persistent migration, as has been shown for pre-aligned collagen networks[20]. Gradients in fiber alignment could also influence local stiffness, which is known to be anisotropic in collagen networks and depend on alignment direction[77]. Recent work has also demonstrated that mechanical pulling and alignment of collagen fibers beyond the leading edge can lead to increases in fiber stiffness and potentially direct cell migration[78]. However, this work does not account for changes in collagen topology or mechanics at the trailing edge, nor does it address the state of the collagen networks in regions directly contacted by cells, as we do in the present study. As gradients in collagen density, stiffness and fiber alignment co-exist and cannot be isolated from one another, it is difficult to identify which gradient plays the most dominant role. Rather, these mechanisms are not mutually exclusive, and it is likely that these simultaneous gradients all contribute to feedback between the substrate perturbation and migration behavior in the cluster that is captured by our theoretical model. Future studies investigating the mechanistic details of such self-generated mechanical gradients will help to shed light on these questions.

In our theoretical model, the nature of the perturbation is not specific and could represent a local change in substrate density, scalar nematic order parameter or substrate stiffness. Although the model makes no assumptions about the precise biological source(s) of the active coupling parameter ζ, this coupling could arise from cellular responses to any or all of these gradients. In addition, our model predicts spontaneous and persistent migration through breaking radial symmetry without a strong dependence on the precise rheological model used. For instance, the linear rheology (Maxwell-like) with a single relaxation time scale could, in principle, be replaced by more complex nonlinear rheological models, provided that they display a comparable relaxation dynamics with finite time scale. In this sense, the main prediction of the model—i.e. that clusters move persistently for large enough relaxation time scales—is very robust and in fact can in principle apply to much more general systems, both living and artificial. The model itself is one-dimensional. However, the mechanism leading to persistent motion (which by essence defines a preferred axis) is robust regardless of the embedding dimensionality, and similar patterns of trailing maximal substrate deformation are expected for 1- 2- or 3-dimensional systems.

Collagen bundling and alignment perpendicular to the tumor edge has been identified as a prognostic marker of cancer invasiveness and is thought to help drive invasive migration in the stroma[19, 79]. Based on our findings, more deformable stromal collagen networks during earlier stages of cancer progression could favor more persistent collective migration. Our rapid cell removal assays showed that relative collagen density relaxed to $\sim$1.5 (Fig. 2h) suggesting that collagen networks are also plastic, consistent with previous findings that cell-scale forces can permanently remodel collagen networks[80]. It is thus possible that repeated collective migration events could lead to

collagen accumulation and increases in network stiffness. However, in the context of cancer, it is much more likely that long-timescale collagen reorganization is driven primarily by cancer associated fibroblasts (CAFs)[33]. Our results indicate that even single CAFs can modify collagen networks more drastically and permanently than large A431 clusters (Extended Data Fig. 9a-c), supporting the idea that stromal reorganization is primarily carried out by CAFs. In the context of cancer, the mechanisms by which tumor cells modify and migrate through the stroma is highly dependent on the the local microenvironment. Future studies further exploring these mechanisms using more complex models and investigating the role of stromal cell remodeling will be crucial for a more complete understanding of cancer cell migration.

Supplementary Note 1: Details on the Theoretical Model

Introduction and summary of the results

We describe here a simple model of cell cluster migration on a viscoelastic substrate, which shows that an apolar cell cluster can perform persistent self propelled motion in absence of any internal self polarization mechanism, and in absence of any external polar cue. The model is general and does not rely on a specific cell type; its aim is to identify the minimal ingredients required for persistent polarized migration of an apolar cell cluster. As we explain below, the main ingredient relies on the active coupling of the apolar cluster to the apolar viscoelastic medium, which we show is sufficient to induce a symmetric breaking in the coupled cluster/substrate system, and thereby persistent motion of the cluster. Our approach is distinct from previous continuum models of cell-substrate interactions[81–83], which have focused on elastic substrates and have imposed a polarity at the cellular level. In our model, symmetry is broken spontaneously, and migration persistence arises from the interactions between cells and their viscoelastic substrate without the need for an imposed polarity component. Motion occurs via a spontaneous symmetry-breaking mechanism that is conceptually similar to a model proposed for autophoretic colloids[39].

In its simplest form, the model first describes the cell cluster as an isotropic active particle, whose position of the center of mass along a reference axis is denoted by x_c. The cluster actively interacts with the underlying viscoelastic substrate: we assume that the cluster, by exerting an active stress on the substrate of intensity prametrized by f, is the source of a scalar structural perturbation $S(x,t)$ in the substrate; without being specific, for a contractile cluster seeded on an ECM-like

fibrilious polymeric substrate, $S(x,t)$ can be a measure of the scalar nematic order parameter in the substrate, and/or a local variation in density.

This perturbation is described phenomenologically in the model and characterized by a relaxation time τ_r and a localization length scale ℓ; this description is based on a minimal description of the substrate rheology as a linear elastic solid (modulus E) with viscous relaxation (viscosity $\eta \propto E\tau_r$).The relaxation time, τ_r is the key parameter in the model that accounts for substrate rheology and can be defined more generally as the ratio of the storage (E) and loss (η) moduli in rheological measurements (i.e. $\tau_r = E/\eta$). Considering more complex rheological models would not qualitatively change the conclusions of the model.

In turn, we assume that the cluster actively responds to the substrate perturbation $S(x,t)$. We do not aim at identifying the microscopic cellular mechanisms involved in this mechanosensitive response, which could be a response to stiffness (i.e. indirectly density) and/or order in the substrate, as was reported at the single cell and cell assemblies levels in various cell types[41,84,85]. Introducing a phenomenological coupling ζ, which parametrizes the active response of the cluster to the perturbation, we write such response in its simplest linear form $v_c = \dot{x}_c = \zeta \partial_x S|_{x_c} + \eta(t)$, where fluctuations can be encoded in a noise term η.

The main results of this model can be summarized as follows : (i) in the absence of noise, a (supercritical) instability occurs for a critical value ζ_c of the activity parameter (with all other parameters held fixed): for $\zeta < \zeta_c$, one has $v_c = 0$, and the cluster cannot migrate persistently; for $\zeta > \zeta_c$, one has $v_c \propto \pm(\zeta - \zeta_c)^{1/2}$. Importantly, we show that the instability threshold scales as

$\zeta_c \sim (f\tau_r)^{-2}$ and is therefore critically controlled by the relaxation time of the gel – at a given level of activity, persistent motion can be enhanced simply by engineering a gel with a τ_r larger than the critical relaxation time τ_c. The dependence on the cluster size L can also be inferred by the model, by noting that both ζ and f are increasing functions of L : persistent motion is therefore predicted to occur only for large enough clusters. (ii) In the presence of noise, the model therefore predicts a Brownian-like random migration with negligible persistence time for $\zeta < \zeta_c$ (or $\tau < \tau_c$), in turn, for $\zeta > \zeta_c$ (or $\tau_r > \tau_c$), it predicts a persistent motion, whose persistence time increases with $\zeta - \zeta_c$, and therefore with τ_r. These results are qualitatively in agreement with experimental observations. A qualitative picture can be useful: by contracting, the cluster effectively induces a local bumpy perturbation in the substrate; in turn, the cluster can slide downhill along the perturbation profile. For a long enough relaxation time of the substrate, the cluster can surf the bump it induces at constant speed. Our model presents a theoretical picture of how a statistically isotropic cell cluster may nevertheless move persistently due to the anisotropy it induces in the substrate as it migrates.

The activity of the cluster induces a perturbation in the substrate, analogous to mechanical forces causing local changes in filament density/orientation/stiffness. For a stationary cluster, both the force from the cluster and the perturbation of the substrate have symmetric profiles around the cluster center, which does not cause any motion. For a cluster moving at speed v_c, because of the viscoelastic relaxation of the substrate, the cluster position is *ahead* of the peak of the substrate deformation profile by $d \sim v_c\tau_r$. This implies that the cluster experiences an active force due to the substrate asymmetry $\propto -\partial_x S$, which increases with d, making it slide downhill along the perturbation profile (assuming $\zeta > 0$ without loss of generality). For small τ_r, the active force is not

sufficient to sustain the speed v_c and the cluster velocity relaxes to 0; however, for large enough τ_r the active force is sufficient to sustain the steady motion at v_c and the particle can surf the deformation profile (which it itself induces) at a constant speed, leading to persistent migration. The model qualitatively recapitulates our initial observations and predicts an offset between the cluster center and deformation peak on the order of the product of the cell velocity and relaxation time ($d \sim v_c\tau_r$). With $v_c = 0.7 \pm 0.4\mu$m/min (Figure 1d) and $\tau_r = 9.1 \pm 6.6$min (Figure 2j), we therefore expect $d = 6.4 \pm 2.6\mu$m. From the average gradient data, the average rearward offset of the collagen density peak is $9.3 \pm 15.2\mu$m, and the average rearward offset of the nematic order minimum is $9.9 \pm 16.2\mu$m, in good agreement with the predictions of the theory.

Last, we provide a general theoretical framework that describes the active dynamics of an apolar system localised in space (the cluster), that we parametrize by a phase field $\phi(x, t)$, which interacts with a generic viscoelastic nematic substrate. This description is fully general, and is shown in particular to encompass the simplest version of the model; its analysis shows that the mechanism leading to persistent motion can be generalized and could be at work in other active systems, living or artificial. Furthermore, this more general model also suggests that larger clusters are more persistent and lead to greater substrate anisotropy, consistent with the experiment.

Minimal model of apolar active particle coupled to a viscoelastic environment

In this section, we write down a simple, one-dimensional heuristic model in which we describe the cell cluster by the position of its centroid x_c. The cell cluster induces a structural perturbation in

the substrate, which we describe by a non-dimensional scalar $S(x,t)$:

$$\partial_t S = -\frac{1}{\tau_r}[S - \ell^2 \partial_x^2 S] + f\delta(x - x_c). \tag{5}$$

Here, the last term on the R.H.S. is the forcing due to the cluster with a strength f which has the dimension of a speed. This equation is derived below in the case where S is the scalar nematic order parameter, or local variation of gel density. The active response of the cluster to the perturbation is written phenomenologically as

$$\dot{x}_c = -\zeta \partial_x S|_{x_c}. \tag{6}$$

We now consider a cluster that moves steadily at speed v_c. Defining $\mu = x - v_c t$, and noting that $x_c = v_c t$, we obtain a pair of self-consistent equations for determining v_c:

$$\left[\frac{1}{\ell^2} - \frac{v_c \tau_r}{\ell^2}\partial_\mu - \partial_\mu^2\right] S = f\frac{\tau}{\ell^2}\delta(\mu) \tag{7}$$

$$v_c = -\zeta \partial_\xi S|_0 \tag{8}$$

From (7), and assuming that S vanishes at large scales, one obtains

$$S(\mu) = -e^{-\frac{\mu(v_c\tau_r + \sqrt{4\ell^2 + v_c^2\tau_r^2})}{2\ell^2}} \frac{f\tau_r}{\sqrt{4\ell^2 + v_c^2\tau_r^2}} \left(e^{-\frac{\mu\sqrt{4\ell^2 + v_c^2\tau_r^2}}{\ell^2}} \Theta[-\mu] + \Theta[\mu] \right), \tag{9}$$

which, when inserted into (8) yields, in addition to $v_c = 0$, the solutions

$$v_c = \pm \frac{\sqrt{f^2\zeta^2\tau_r^4 - 16\ell^6}}{2\ell^2\tau_r}. \tag{10}$$

This has the form

$$v_c = \pm \frac{f\tau_r}{2\ell^2}\sqrt{\zeta^2 - \zeta_c^2} \tag{11}$$

where $\zeta_c = 4\ell^3/f\tau_r^2$. That is, as a function of the activity parameter, v_c undergoes a supercritical pitchfork bifurcation at ζ_c and assumes a non-zero value. Eq. (11) implies that when $\zeta \gg \zeta_c$, $v_c \sim \zeta$. When all other quantities are held constant, $v_c \sim \tau_r$ at large τ_r and $v_c \sim 1/\ell^2$.

So far we assumed that the forcing of the polymeric substrate due to the cell cluster is localised purely at the centroid of the cluster. We now relax this hypothesis and demonstrate that the basic mechanism leading to the instability remains correct even when the source of the perturbation $\delta(x - x_c)$ in (5) is not localized, but replaced by a general function $g(x - x_c)$ peaked at x_c and vanishing at large scales, and with its integral normalized to 1. That is,

$$\partial_t S = -\frac{1}{\tau_r}[S - \ell^2 \partial_x^2 S] + f g(x - x_c). \tag{12}$$

Importantly, g is assumed to be even, meaning that the cluster has no intrinsic polarity. We assume that $\int_{-\infty}^{\infty} g(y)dy = 1$. To reduce the number of parameters, we now rescale space by ℓ i.e., define $\tilde{x} = x/\ell$ and time by τ_r, i.e. $\tilde{t} = t/\tau_r$. Further, defining $\xi = \tilde{x} - \bar{v}_c\tilde{t}$, where $\bar{v}_c = v_c\tau/\ell$, we get the equations of motion

$$\left[-1 + \bar{v}_c\partial_\xi + \partial_\xi^2\right] S = -\tilde{f} g(\xi) \tag{13}$$

where $\tilde{f}$ is the non-dimensionalised version of f and depends linearly on τ_r, $g(\xi)$ is a non-dimensionalised version of the function $g(x - x_c)$ and

$$\bar{v}_c = -\tilde{\zeta}\partial_\xi S|_0 \tag{14}$$

where $\tilde{\zeta} = \zeta\tau_r/\ell^2$. We can now solve (13) using the Green's function

$$\mathcal{G}(\xi, \xi') = -\frac{1}{\sqrt{\bar{v}_c^2 + 4}} e^{\frac{\xi - \xi'}{2}(-\bar{v}_c + \sqrt{\bar{v}_c^2+4})} \left[e^{(\xi' - \xi)\sqrt{\bar{v}_c^2+4}}\Theta(\xi - \xi') + \Theta(\xi' - \xi)\right]. \tag{15}$$

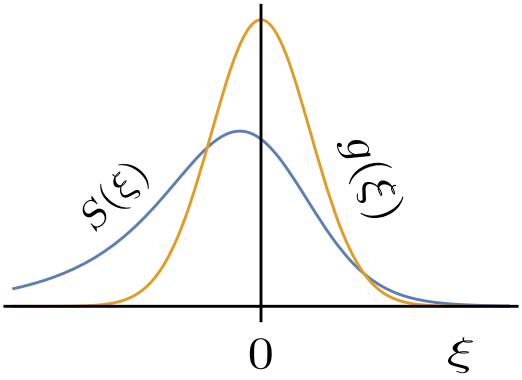

Supplementary Fig. 1: The cluster induces a symmetric contractile stimulus g localized at the cluster centre which is expected to peak at x_c and vanish for $x - x_c \gg 0$. Because of the finite relaxation time τ_r, the response of the substrate (perturbation S) is delayed. For a moving cluster, this delay causes a space shift and asymmetry of the perturbation S.

with $S(\xi) = \tilde{f} \int_\infty^\infty \mathcal{G}(\xi, \xi') g(\xi')$. The speed can then be calculated as

$$\bar{v}_c = \tilde{\zeta} \partial_\xi S|_0 = \tilde{\zeta} \partial_\xi \int_{-\infty}^{\infty} \mathcal{G}(\xi, \xi') \tilde{f} g(\xi') d\xi'|_0 = \tilde{\zeta} \int_{-\infty}^{\infty} \partial_\xi [\mathcal{G}(\xi, \xi')] \tilde{f} g(\xi') d\xi'|_0. \tag{16}$$

Here,

$$\partial_\xi [\mathcal{G}(\xi, \xi')] = -\frac{1}{\sqrt{4 + \bar{v}_c^2}} e^{\frac{-\bar{v}_c + \sqrt{4+\bar{v}_c^2}}{2}(\xi - \xi')} \left[\left\{ e^{\sqrt{4+\bar{v}_c^2}(\xi' - \xi)} - 1 \right\} \delta(\xi - \xi') - \frac{\bar{v}_c + \sqrt{4 + \bar{v}_c^2}}{2} e^{\sqrt{4+\bar{v}_c^2}(\xi' - \xi)} \Theta(\xi - \xi') + \frac{-\bar{v}_c + \sqrt{4 + \bar{v}_c^2}}{2} \Theta(\xi' - \xi) \right]. \tag{17}$$

Using this, one obtains

$$\bar{v}_c = \tilde{\zeta} \int_{-\infty}^{\infty} \frac{e^{\frac{\bar{v}_c - \sqrt{4+\bar{v}_c^2}}{2} \xi'} \left[(\bar{v}_c + \sqrt{4 + \bar{v}_c^2}) e^{\sqrt{4+\bar{v}_c^2} \xi'} \Theta(-\xi') + (\bar{v}_c - \sqrt{4 + \bar{v}_c^2}) \Theta(\xi') \right]}{2\sqrt{4 + \bar{v}_c^2}} \tilde{f} g(\xi') d\xi'. \tag{18}$$

Since the kernel in (18) is not symmetric under $\xi' \to -\xi'$, a function $g(\xi')$ which is symmetric

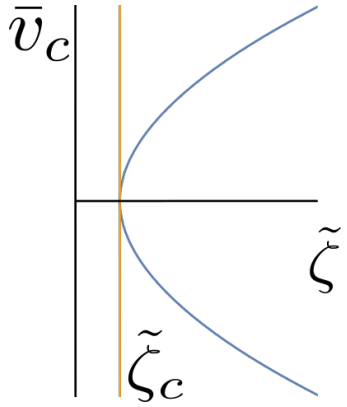

Supplementary Fig. 2: $\bar{v}_c$ undergoes a supercritical pitchfork bifurcation at $\tilde{\zeta} = \tilde{\zeta}_c$. Here, $\bar{v}_c$ is plotted as a function of $\tilde{\zeta}$ for $g(\xi') = e^{-\xi'^2/2}/\sqrt{2\pi}$.

and has a maximum at $\xi' = 0$ should yield a non-zero value of the integral. See Supplementary Fig. 1 for an example. Since we demand that $g(\xi')$ has a maximum at $\xi' = 0$, $g(\xi')$ must remain (at least) finite as $|\xi'| \to \infty$. The value of the integral is finite for all such $\tilde{f}(\xi')$. Furthermore, since the integral goes to 0 as $|\bar{v}_c| \to \infty$, a nontrivial (non-zero) solution of the self-consistent equation for $\bar{v}_c$, (18) *must* exist when the slope of the R.H.S. of (18) with respect to $\bar{v}_c$ exceeds 1 at $\bar{v}_c = 0$. That is, the cluster spontaneously transitions to a symmetry-broken steadily-moving state beyond a critical activity $\tilde{\zeta}_c$ given by

$$\frac{4}{\tilde{\zeta}_c} = \int_{-\infty}^{\infty} \tilde{f} g(\xi') \left[e^{\xi'}(1+\xi')\Theta(-\xi') + e^{-\xi'}(1-\xi')\Theta(\xi) \right] d\xi' \tag{19}$$

Notice that the integral on the R.H.S. does not diverge for any reasonable function which has unique maximum at $\xi' = 0$. (Notice that the term in the square bracket vanishes as $|\xi'|e^{-|\xi'|}$ as $|\xi'| \to \infty$.) This equation therefore always has a solution – again implying that there is always a critical (non-zero) $\tilde{\zeta}_c$ beyond which the cell cluster starts moving, *irrespective* of the precise form of the forcing function $g(\xi)$. We can also infer the scaling of $\tilde{\zeta}_c$ on τ_r directly from this:

$\tilde{f} \sim .f\tau_r$ which implies $\tilde{\zeta}_c \sim (f\tau_r)^{-1}$ and using the definition of $\tilde{\zeta}$, $\zeta_c \sim (f\tau_r)^{-2}$ as given in the main text. We demonstrate the supercritical bifurcation diagram implied by (18) for a profile with $g(\xi) = e^{-\xi^2/2}/\sqrt{2\pi}$ with $\tilde{f} = 1$ in Supplementary Fig. 2.

It is difficult to directly read-off the exact dependence of the speed of the cluster on τ_r and ℓ as it depends on the form of the forcing function. To show this explicitly, we revert to the dimensional variables and write the fully dimension restored version of (18):

$$v_c = \frac{\zeta f \tau_r}{\ell^2} \int_{-\infty}^{\infty} d\mu' g(\mu') \frac{e^{-\frac{\mu'\left(-v_c\tau_r + \sqrt{4\ell^2 + v_c^2\tau_r^2}\right)}{2\ell^2}}}{2\sqrt{4\ell^2 + v_c^2\tau_r^2}} \left[e^{\frac{\mu'\sqrt{4\ell^2+v_c^2\tau_r^2}}{\ell^2}} \left(v_c\tau_r + \sqrt{4\ell^2 + v_c^2\tau_r^2} \right) \Theta(-\mu') + \left(v_c\tau_r - \sqrt{4\ell^2 + v_c^2\tau_r^2} \right) \Theta(\mu') \right] \quad (20)$$

where $\mu = x - v_c t$ as defined earlier. It is clear that the detailed dependence of the solution of this equation on τ_r is complicated, in general. We now specialise to a Gaussian profile for $g(\mu) \equiv e^{-\mu^2/2\sigma^2}/\sqrt{2\pi}\sigma$ such that we recover the results we obtained for the δ function forcing when $\sigma \to 0$. In this case, the condition for the cluster motility becomes

$$\frac{f\zeta\tau_r^2}{2\sqrt{2\pi}\ell^5} \left[-2\ell\sigma + e^{\frac{\sigma^2}{2\ell^2}} \sqrt{2\pi}(\ell^2 + \sigma^2) \text{erfc}\left(\frac{\sigma}{\sqrt{2}\ell} \right) \right] > 1. \quad (21)$$

This clearly implies that increasing the relaxation time τ_r or the activity ζ promotes the motility of the cluster and the critical activity $\zeta_c \sim \tau_r^2$. In other words, if we increase τ_r without modifying any other parameter, at a finite $\tau_r = \tau_c$ a $v_c \neq 0$ solution sets in and the particle starts moving spontaneously. We have checked that this conclusion is unmodified even for more general forcing functions.

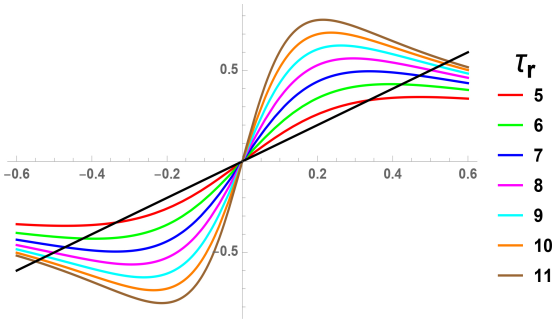

(a) Solutions of (20) with $\ell = 1$, $\zeta = 1$, $f = 1$, and $\sigma = 1$

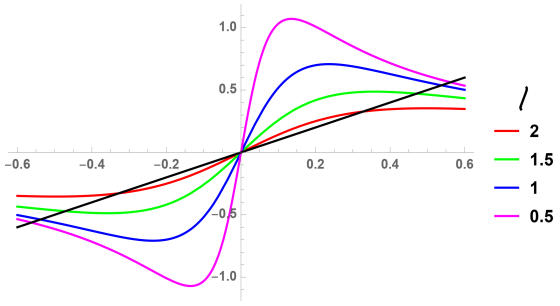

(b) Solutions of (20) with $\tau_r = 10$, $\zeta = 1$, $f = 1$, and $\sigma = 1$

Supplementary Fig. 3: The solutions of (20) for multiple ℓ and τ_r; the intersection of the black straight line with the curves for different τ_r is the solution of v_c for that τ_r. This demonstrates that v_c increases with τ_r before asymptotically going to a constant value. Similarly, it decreases with ℓ and asymptotically goes to a constant value for large ℓ.

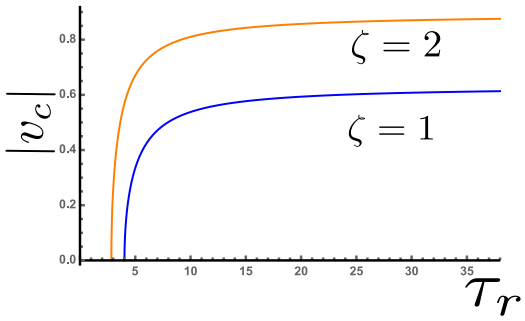

Supplementary Fig. 4: v_c as a function of τ_r with $\ell = 1$, $f = 1$ and $\sigma = 1$. This demonstrates that as τ_r increases, v_c goes to a constant value.

Unfortunately, the solution of the self-consistent equation cannot be obtained in a closed form even for a Gaussian forcing function. Therefore, we present its graphical solution in Supplementary Fig. 3 for a Gaussian profile with $\sigma = 1$ for multiple τ_r and ℓ, holding $\zeta = 1$ and $f = 1$ fixed. We explicitly calculate the scaling of v_c with τ_r in Supplementary Fig. 4 and demonstrate that it goes to a ζ-dependent constant as τ_r increases. This is therefore consistent with v_c being controlled by ζ with τ_r entering *only* through the dependence of ζ_c on it. This conclusion is reasonable in a biological context, since one cannot increase the speed of a cluster arbitrarily simply by increasing the correlation time of the medium of the substrate. The conclusion is also consistent with the results obtained in the experiments. Eq. (11) implied that for a delta-function, v_c scales as ζ for large ζ. We recover this result for a Gaussian profile with $\sigma \to 0$. However, for larger σ, this continuously changes with $v_c \sim \sqrt{\zeta}$ as we show in Supplementary Fig. 5. In fact, for Gaussian profiles with $\sigma \approx 1$, the activity acts like temperature in a usual second-order phase transition, like in the Ising model. We show that $\zeta - \zeta_c$ scales as v_c^2 in Supplementary Fig. 6 which implies that $v_c \sim \sqrt{\zeta - \zeta_c}$ as noted in the main text.

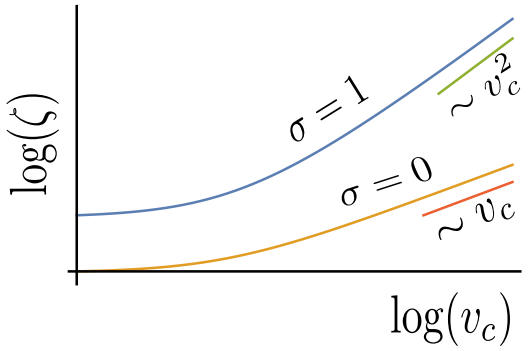

Supplementary Fig. 5: At large v_c, $\zeta \sim v_c^2$ for Gaussian distributions with $\sigma = 1$ and $\zeta \sim v_c$ for delta function distributions ($\sigma = 0$) for $f = 1$, $\ell = 1$ and $\tau_r = 1$. This implies that $v_c \sim \sqrt{\zeta}$ for large ζ for Gaussian profiles with $\sigma = 1$ in contrast to $v_c \sim \zeta$ for a δ-function forcing.

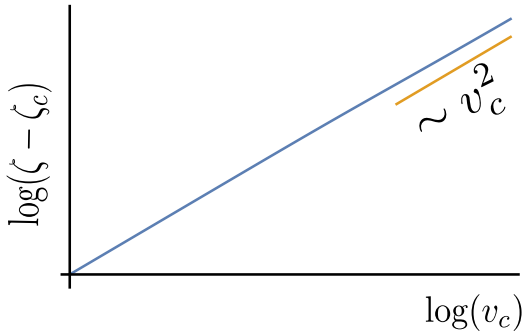

Supplementary Fig. 6: $\zeta - \zeta_c$ as a function of v_c for $f = 1$, $\ell = 1$ and $\tau_r = 1$. This demonstrates that $v_c \sim \sqrt{\zeta - \zeta_c}$.

The fact that $v_c \sim \sqrt{\zeta - \zeta_c}$ and that τ_r and ℓ only affects ζ_c implies that we can heuristically view this as a phase transition controlled by a potential of the form $U = av^2/2 + bv^4/4$ with $a \propto \zeta_c - \zeta$. For $\zeta > \zeta_c$, i.e. for $a < 0$, the expectation value of v, $\langle v \rangle = v_c = \sqrt{-a/b} \propto \sqrt{\zeta - \zeta_c}$ and the potential has a double well with the minimum $U_{\text{min}} = -a^2/2b = -bv_c^2/2 \propto \zeta - \zeta_c$. This allows us to estimate the time before a motile cluster ($|v_c| > 0$) reverses its direction of motility (recall, that the direction of motility is determined by the sign of v_c) – within this heuristic potential picture, this corresponds to the crossing of a barrier of height $\Delta U = bv_c^2/2 \propto \zeta - \zeta_c$. Consider a noise of strength $2D$ that affects the dynamics of the cluster – Eq. (8) needs to be supplemented with a white noise with a variance $2D$ for this – the escape time from a potential of depth ΔU is then $\tau_e \propto e^{\Delta U/D}$. This implies that $\tau_e \sim e^{v_c^2} \sim e^{\zeta - \zeta_c}$. Therefore, at a constant value of ζ, increasing τ_r decreases ζ_c and leads to an *increase* of τ_e. However, τ_e goes to a constant for large τ_r (since v_c goes to a constant as well). We have however assumed that the noise strength and the relaxation time τ_r of the medium can be tuned independently. This may not be the case for the experiments and a more accurate prediction of the escape time requires a more detailed description of the noise. However, it is gratifying that even this impressionistic description manges to reproduce the qualitative feature that increasing the relaxation time leads to an increase of the escape time and therefore, cell clusters move unidirectionally more persistently. Moreover, while the detailed scaling of τ_e with respect to $\zeta - \zeta_c$ depends on the form of the forcing function, the scaling with respect to v_c holds irrespective of the forcing function. Since v_c is expected to increase with τ_r, at least for intermediate values of τ_r, the persistence time of the cluster is expected to generally increase with τ_r.

Connection with a more detailed description of an isotropic motile layer

To connect this simple picture of motility described in the previous section to a more detailed theory of a cluster described as an active droplet, we now describe the moving cluster by a phase field $\phi(\mathbf{x}, t)$, with $\phi = 1$ describing the interior of the cluster. The velocity field of the cluster is denoted by $\mathbf{v}(\mathbf{x}, t)$. The anisotropy of the the substrate is described by the apolar tensor $\mathbf{Q}(\mathbf{x}, t)$. The equation for the phase field is

$$\dot{\phi} + \nabla \cdot (\mathbf{v}\phi) = \nabla^2 \frac{\delta F}{\delta \phi} \tag{22}$$

where F is the usual phase-field free energy. The overdamped equation for the velocity field is phenomenologically taken to be

$$\mathbf{v} = [\zeta_0 \mathbf{I} + \zeta_1 \mathbf{Q}] \cdot \nabla\phi - [M_0 \mathbf{I} + M_1 \mathbf{Q}] \cdot \phi \nabla \frac{\delta F}{\delta \phi} \tag{23}$$

where we have used an anisotropic mobility $[M_0\mathbf{I} + M_1\mathbf{Q}]$ with $\mathbf{I}$ being the identity tensor. ζ_0 and ζ_1 are active coefficients. The anisotropy of the substrate is affected by the motion as well as the shape of the cluster:

$$\dot{\mathbf{Q}} = -[\alpha - D\nabla^2]\mathbf{Q} + \lambda_0[\nabla\phi\nabla\phi - (1/2)(\nabla\phi)^2\mathbf{I}] + \lambda_1[\nabla\nabla\phi - (1/2)\nabla^2\phi\mathbf{I}] + \mu_0[\mathbf{vv} - (1/2)|\mathbf{v}|^2\mathbf{I}] + \mu_1[\nabla\mathbf{v} + (\nabla\mathbf{v})^T - \nabla\cdot\mathbf{v}\mathbf{I}]. \tag{24}$$

The first direct term on the R.H.S. is the relaxation of the substrate when there is no aligning effect due to the cluster. The terms with the coefficients λ_0 and λ_1 describe the modification of the surface anisotropy due to the shape of the cluster (these terms can appear from free energy couplings $\mathbf{Q} : \nabla\phi\nabla\phi$ and $\mathbf{Q} : \nabla\nabla\phi$). The μ_1 term describes usual flow-alignment. The term with

the coefficient μ_0 is more complicated. It exists only in systems on substrates but may be present *even* in passive systems where it can arise from a free energy term $\mathbf{Q} : \mathbf{vv}$. We want to check whether the cluster can *spontaneously* break symmetry and acquire a non-zero average velocity $\langle \mathbf{v} \rangle$ in some direction we denote by $\hat{x}$. For simplicity, we also assume that all variations are only in this direction and reduce the two-dimensional problem to a one-dimensional one, i.e. $\phi \equiv \phi(x,t)$, $\mathbf{v} \equiv v_x(x,t)$. In this spirit, we assume that the apolar order parameter is

$$\mathbf{Q} = S(x) \begin{pmatrix} 1 & 0 \\ 0 & -1 \end{pmatrix} \tag{25}$$

This leads to the equations

$$\partial_t \phi + v_x \partial_x \phi = \partial_x^2 \frac{\delta F}{\delta \phi} \tag{26}$$

$$v_x = [\zeta_0 + \zeta_1 S] \partial_x \phi - [M_0 + M_1 S] \phi \partial_x \frac{\delta F}{\delta \phi} \tag{27}$$

$$\partial_t S = -[\alpha - D\partial_x^2] S + \frac{\lambda_0}{2} (\partial_x \phi)^2 + \frac{\lambda_1}{2} \partial_x^2 \phi + \frac{\mu_0}{2} v_x^2 + \mu_1 \partial_x v_x. \tag{28}$$

We now look at a drop which has fixed shape due to a high stiffness such that $\phi \approx 0$ outside a small region. We assume $\delta F / \delta \phi \approx 0$. We take ϕ to be ≈ 1 between L and $-L$ and 0 outside it. In this case, the average velocity of the cluster is

$$v_c = \frac{1}{2L} \int_{-L}^{L} v_x(x) dx. \tag{29}$$

This implies

$$v_c = \frac{\zeta_0}{2L} \int_{-L}^{L} \partial_x \phi dx + \frac{\zeta_1}{2L} \int_{-L}^{L} S(x) \partial_x \phi dx = \zeta_1 [S(x)\phi(x)]_{-L}^{L} - \frac{\zeta_1}{2L} \int_{-L}^{L} \phi(x) \partial_x S dx. \tag{30}$$

This implies

$$v_c = -\zeta_1 \frac{S(L) - S(-L)}{2L}. \tag{31}$$

In the limit $L \to 0$, $-\lim_{L\to 0} \zeta_1 S(L) - S(-L)/2L = -\zeta_1 \partial_x S|_{x_c}$. In the $S(x)$ equation, the velocity couplings lead to nonlinear terms in $S(x)$ or modify the coefficients λ_0 and λ_1. Therefore, the ordering is induced primarily by the terms $(\partial_x \phi)^2$ and $\partial_x^2 \phi$. Both of these terms are even functions of x about 0 for a ϕ profile that is an even function of x. These dynamical equations are equivalent to the ones we we considered in the last section and results in the same spontaneous symmetry-breaking transition mechanism discussed there. This demonstrates that a less impressionistic model of a cell-cluster reduces to the more impressionistic version of a point particle in a self-generated deformation field and justifies its consideration to provide a qualitative understanding of the experimental phenomenon.

Interpretation of the structural perturbation S in the model

In the main text, we declared that the S field can describe both a perturbation of the apolar organisation of the collagen filaments as well as the local density of the collagen. The first is obvious – S in this case is the norm of the rank-2 apolar order parameter tensor and measures the local degree of apolar orientation. In the isotropic phase, the viscous relaxation dynamics of S is generically given by Eq. 5[86]. However, the second requires more explanation not the least because density is a conserved variable and must be associated with a continuity equation. We now provide an interpretation of the equation of motion for S to clarify this. Consider a slab geometry in which the collagen network of thickness h rests on a solid substrate to which it is pinned. The

cluster is on the top surface of the collagen network. We allow for only transverse displacements of the collagen network. Then, the overdamped dynamics of the displacement field $\mathbf{u}_\perp$ must be $\gamma\partial_t\mathbf{u}_\perp = \lambda\nabla\mathbf{u}_\perp + \mu\nabla_\perp\nabla_\perp\cdot\mathbf{u}_\perp$ where γ is a friction coefficient and λ and μ are the shear and bulk modulus respectively ($\propto E$ in the main text). Note that $\mathbf{u}_\perp$ is a function of both the transverse, in plane variables, x, y and the vertical one z where z is the coordinate that is measured from the bottom of the collagen layer with the network being pinned to the solid below it at $z = 0$ i.e., $\mathbf{u}_\perp(z = 0) = 0$. Therefore,

$$\gamma\partial_t\mathbf{u}_\perp = \lambda\nabla_\perp^2\mathbf{u}_\perp + \lambda\partial_z^2\mathbf{u}_\perp + \mu\nabla_\perp\nabla_\perp\cdot\mathbf{u}_\perp + \tilde{f}g(x - x_c)\delta(z - h) \tag{32}$$

where the last term denotes the forcing due to the cluster. We can now average this over the thickness of the network. This will generically yield

$$\gamma\partial_t\bar{\mathbf{u}}_\perp = \lambda\nabla_\perp^2\bar{\mathbf{u}}_\perp - \xi\frac{\lambda}{h^2}\bar{\mathbf{u}}_\perp + \mu\nabla_\perp\nabla_\perp\cdot\bar{\mathbf{u}}_\perp + \xi_2\tilde{f}hg(x - x_c) \tag{33}$$

where $\bar{\mathbf{u}}_\perp$ is the averaged displacement field and ξ and ξ_2 are dimensionless numbers > 0 whose exact value depends on the displacement profile in z. It might appear surprising at first glance that while (32) is manifestly invariant under $\mathbf{u}_\perp \to \mathbf{u}_\perp + \text{const.}$, (33) is not – i.e., it loses *translation* invariance. This is a consequence of the pinning of the collagen layer to the solid at the bottom – this pinning fixes a preferred reference frame for the displacement field. Now, in the spirit of the one-dimensional model we allow for displacement only in $\hat{x}$ direction, i.e. only $\bar{u}_x$ is non-zero, and allow *that* to vary only along x, which yields

$$\gamma\partial_t\bar{u}_x = (\lambda + \mu)\partial_x^2\bar{u}_x - \xi\frac{\lambda}{h^2}\bar{u}_x + \xi_2\tilde{f}hg(x - x_c) \tag{34}$$

Identifying $\bar{u}_x$ with S, $\gamma h^2/(\xi\lambda)$ with τ_r, $h^2(\lambda+\mu)/(\xi\lambda)$ with ℓ^2 and $\xi_2\tilde{f}/\gamma$ with f, we can map this model onto (12). Since in a crosslinked gel, the dynamics of density fluctuations $\delta\rho$ is slaved to the displacement dynamics via $\partial_t(\delta\rho + \nabla_\perp \cdot \mathbf{u}_\perp) = 0$, which with the assumptions we have made can be rewritten as $\partial_t(\delta\rho + \partial_x \bar{u}_x) = 0$, this interpretation provides direct information about the density fluctuations as well.

Now we come to how the phenomenological coefficients in these equations are modified when the collagen gel gets more crosslinked. In the interpretation in which S is the scalar orientational order parameter, crosslinking is likely to *reduce* τ_r while not significantly affecting ℓ since random crosslinking is likely to *hinder* orientational ordering. This, as discussed in the main text, leads to a *decrease* of persistent motion. In the interpretation in which S is identified with the displacement field $\bar{u}_x$, $\tau_r = \gamma h^2/(\xi\lambda)$. Since crosslinking *increases* the stiffness of the network, which should *increase* the shear modulus, τ_r is again reduced and ℓ^2, which is controlled by the ratio of bulk and shear moduli is not likely to be significantly affected. This implies that again in this interpretation, crosslinking should *reduce* the directed motion of the cluster.

Supplementary References

65. Chan, C. E. & Odde, D. J. Traction dynamics of filopodia on compliant substrates. *Science* **322**, 1687–1691 (2008).

66. Elosegui-Artola, A. *et al.* Mechanical regulation of a molecular clutch defines force transmission and transduction in response to matrix rigidity. *Nat. Cell. Biol.* **18**, 540–548 (2016).

67. Cantini, M., Rico, P., Moratal, D. & Salmerón-Sánchez, M. Controlled wettability, same chemistry: biological activity of plasma-polymerized coatings. *Soft Matter* **8**, 5575–5584 (2012).

68. Tweedy, L., Knecht, D. A., Mackay, G. M. & Insall, R. H. Self-generated chemoattractant gradients: Attractant depletion extends the range and robustness of chemotaxis. *PLoS Biol.* **14**, e1002404– (2016).

69. Ramel, D., Wang, X., Laflamme, C., Montell, D. J. & Emery, G. Rab11 regulates cell-cell communication during collective cell movements. *Nat. Cell. Biol.* **15**, 317–324 (2013).

70. d'Alessandro, J. *et al.* Cell migration guided by long-lived spatial memory. *Nat. Commun.* **12**, 4118 (2021).

71. Panneerselvam, M., Sahai, A. & Salomon, D. S. Modulation of type-IV procollagen and laminin production in A431 human squamous epidermoid carcinoma cells by 12-o-tetradecanoylphorbol-13-acetate (TPA) and epidermal growth factor (EGF). *Arch. Dermatol.* **277**, 377–383 (1985).

72. Sapudom, J. *et al.* The interplay of fibronectin functionalization and TGF-β1 presence on fibroblast proliferation, differentiation and migration in 3D matrices. *Biomater. Sci.* **3**, 1291–1301 (2015).

73. Dechantsreiter, M. A. *et al.* N-methylated cyclic RGD peptides as highly active and selective $\alpha_{\mathrm{V}}\beta_3$ integrin antagonists. *J. Med. Chem.* **42**, 3033–3040 (1999).

74. Hall, D. E. *et al.* The α_1/β_1 and α_6/β_1 integrin heterodimers mediate cell attachment to distinct sites on laminin. *J. Cell Biol.* **110**, 2175–2184 (1990).

75. Lo, C. M., Wang, H. B., Dembo, M. & Wang, Y. L. Cell movement is guided by the rigidity of the substrate. *Biophys. J.* **79**, 144–152 (2000).

76. Novikova, E. A., Raab, M., Discher, D. E. & Storm, C. Persistence-driven durotaxis: Generic, directed motility in rigidity gradients. *Phys. Rev. Lett.* **118**, 078103– (2017).

77. Goren, S., Koren, Y., Xu, X. & Lesman, A. Elastic anisotropy governs the range of cell-induced displacements. *Biophys. J.* **118**, 1152–1164 (2020).

78. van Helvert, S. & Friedl, P. Strain stiffening of fibrillar collagen during individual and collective cell migration identified by afm nanoindentation. *ACS Appl. Mater. Interfaces* **8**, 21946–21955 (2016).

79. Clark, A. G. & Vignjevic, D. M. Modes of cancer cell invasion and the role of the microenvironment. *Curr. Opin. Cell Biol.* **36**, 13–22 (2015).

80. Mohammadi, H., Arora, P. D., Simmons, C. A., Janmey, P. A. & McCulloch, C. A. Inelastic

behaviour of collagen networks in cell–matrix interactions and mechanosensation. *J. R. Soc. Interface* **12**, 20141074 (2015).

81. Banerjee, S. & Marchetti, M. C. Substrate rigidity deforms and polarizes active gels. *EPL* **96**, 28003 (2011).

82. Banerjee, S. & Marchetti, M. C. Contractile stresses in cohesive cell layers on finite-thickness substrates. *Phys. Rev. Lett.* **109**, 108101 (2012).

83. Banerjee, S. & Marchetti, M. C. Controlling cell-matrix traction forces by extracellular geometry. *New J. Phys.* **15**, 035015 (2013).

84. Pelham, R. J. & Wang, Y.-l. Cell locomotion and focal adhesions are regulated by substrate flexibility. *Proc. Natl. Acad. Sci. USA* **94**, 13661 (1997).

85. Charras, G. & Sahai, E. Physical influences of the extracellular environment on cell migration. *Nat. Rev. Mol. Cell Biol.* **15**, 813–824 (2014).

86. de Gennes, P. G. & Prost, J. *The Physics of Liquid Crystals*, vol. 2 (Oxford Univ. Press, Oxford, 1993).